Metal–metal interactions in dinuclear ruthenium complexes containing bridging 4,5-di(2-pyridyl)imidazolates and related ligands†

Jonathan W. Slater,[a] Deanna M. D'Alessandro,[b] F. Richard Keene[b] and Peter J. Steel*[a]

Received 21st October 2005, Accepted 20th December 2005
First published as an Advance Article on the web 12th January 2006
DOI: 10.1039/b514976m

The dinuclear bis(2,2′-bipyridine)ruthenium complex of 4,5-di(2-pyridyl)imidazolate has been prepared and separated into its (*meso* and *rac*) diastereoisomers. The 2-phenyl substituted analogue forms the *meso* isomer selectively. All three complexes have been characterised by ^{1}H NMR and X-ray crystallography. Electrochemical measurements and spectroelectrochemistry of the mixed-valence states reveal strong metal–metal interactions and IVCT bands that are highly dependent on the electrolyte.

Introduction

For several decades, ligand-mediated metal–metal interactions have been the subject of extensive study in a variety of contexts, ranging from pure inorganic to applied biological chemistry. Much of this effort has been centred on bridging nitrogen-containing heterocyclic ligands, which are well known to facilitate interactions between metal atoms through the π-system of the ligand.[1–3] Within this context ruthenium complexes of doubly-chelating bridging ligands have been particularly well studied.[2] For example, 2,2′-bipyrimidine (**1**) and 2,2′-azobis(pyridine) (**2**) (Fig. 1) both chelate to two metal centres and have been shown to demonstrate strong inter-metal interactions, which are particularly strong for complexes of (**2**).[4,5] Numerous other bridging ligands have been reported and various explanations have been forwarded to explain the magnitude of the communication between the metal centres. Factors such as the metal–metal distance, the degree of conjugation between the metal centres and the electronic properties of the ligand and metals are generally accepted as being important.[1,2] Nevertheless, there still remains much uncertainty as to what really mediates these effects.

As part of a programme involving the study of new bridging ligands,[6] we described the preparations and complexes of two ligands, (**3**) and (**4**), incorporating 1,2,5-oxadiazole and 1,2,5-thiadiazole bridging subunits.[7] Electrochemical studies of dinuclear ruthenium complexes of these ligands revealed remarkably strong metal–metal interactions, greater than those found in the corresponding complexes of (**1**), despite the greater inter-metal separation, and greater than those previously reported in complexes of 2,3-di(2-pyridyl)pyrazine (**5**)[8] and 4,6-di(2-pyridyl)pyrimidine (**6**)[9] despite the obvious similarities in geometry. Furthermore, we observed an intriguing difference between the magnitude of the metal–metal interactions for the two diastereoisomeric (*meso* and *rac*) forms of the dinuclear complexes containing the Ru(bpy)$_2$ terminal moieties (bpy = 2,2′-bipyridine).[7] Table 1 summarises these previous reports.

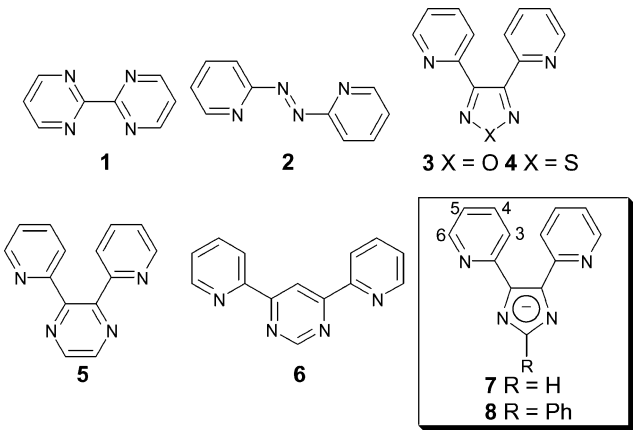

Fig. 1 Bridging doubly-chelating ligands.

Table 1 K_c values for dinuclear Ru(bpy)$_2$ complexes of **(1)–(6)**

Compound	K_c[a]
1*rac*[b]	1510
1*meso*[b]	1760
2*rac*[c]	283 000 000
2*meso*[c]	192 000 000
3*rac*[d]	480 000
3*meso*[d]	1 220 000
4*rac*[d]	23 000
4*meso*[d]	29 000
5[e]	747
6[e]	506

[a] Comproportionation constant, $K_c = \exp\{\Delta E_{ox} F/RT\}$, where F/RT takes the value 38.92 V^{-1}, in $[(n\text{-}C_4H_9)_4N]PF_6$–$CH_3CN$ at 298 K. [b] Values from ref. 4*c*. [c] Ref. 5*d*. [d] Ref. 8. [e] Ref. 9.

In search of an explanation for the origin of this amplified communication between the metals and to ascertain whether the presence of a heteroatom in the ligand facilitates this increased interaction, we have synthesised a number of structurally-related bridging ligands for investigation. Here we report the synthesis and electrochemical properties of dinuclear ruthenium complexes of two 4,5-di(2-pyridyl)imidazolates, (**7**) and (**8**), which contain carbon atoms in place of the oxygen/sulfur atoms of the central

[a]*Department of Chemistry, University of Canterbury, Christchurch, New Zealand. E-mail: peter.steel@canterbury.ac.nz*
[b]*School of Pharmacy & Molecular Sciences, James Cook University, Townsville, Queensland, 4811, Australia*

† Electronic supplementary information (ESI) available: UV/Vis/NIR data for **3**$^{n+}$, **4**$^{n+}$ and **9**$^{n+}$; NIR data for **3**$^{5+}$, **4**$^{5+}$ and **9**$^{4+}$; overlay of the spectra for **9*rac***$^{n+}$; quantitative MO diagram for the $[\{Ru(bpy)_2\}_2(\mu\text{-BL})]^{5+}$ systems. See DOI: 10.1039/b514976m

 This journal is © The Royal Society of Chemistry 2006

ring, along with spectroelectrochemical studies of these and related complexes.

Results and discussion

Ligand syntheses

4,5-Diaryl-1*H*-imidazoles are readily prepared by reaction of a 1,2-diketone with the appropriate aldehyde in the presence of a large excess of ammonium acetate in acetic acid. The preparations of the protonated forms of (**7**)[10] and (**8**)[11] have previously been described using this method, albeit in low yields. During the course of our work a more efficient synthetic route to 1*H*-imidazoles was reported[12] that utilises microwave irradiation. We found that this method eliminated the problem of side products being formed and resulted in improved yields. In this way the parent imidazole (**7**) was prepared from the reaction of 2,2′-pyridil and hexamethylenetetramine as a source of formaldehyde. The 2-phenyl derivative (**8**) was prepared similarly from reaction between 2,2′-pyridil and benzaldehyde. In both cases using a solely thermal method resulted in the formation of significant amounts of a second major product possessing a fused imidazolo[1,5-*a*]pyridine ring system.[11]

The ligands were unambiguously characterised by NMR and mass spectrometry. An interesting feature of the NMR spectra of both compounds was the broad nature of the peaks corresponding to the four pyridyl protons. Although prototropic tautomerism of 1*H*-imidazoles is normally fast on the NMR time-scale,[13] this process is substantially slowed in the present compounds due to intramolecular hydrogen bonding between the NH hydrogen and the adjacent pyridyl nitrogen, thereby explaining the broadening of the pyridyl signals. In contrast, sharp signals are observed for the proton in the 2-position in (**7**) and the three peaks corresponding to the five phenyl protons in (**8**), which are not subject to symmetrisation by the tautomerism process.

Ruthenium complexes of (7) and (8)

Dinuclear ruthenium complexes of both the bridging ligands were conveniently synthesised from the reaction of two equivalents of $[Ru(bpy)_2Cl_2]\cdot 2H_2O$ and the appropriate ligand. We have found a microwave-assisted method to give the shortest reaction times and the cleanest reaction products. Using this technique, reactions were carried out in ethylene glycol, with the addition of a small amount of sodium hydroxide to deprotonate the ligand, to afford the desired dinuclear products in high yields. The two diastereoisomers (**9*rac***) and (**9*meso***) were readily separated by column chromatography, using a method which was pioneered in one of our laboratories,[14] employing SP Sephadex C-25 and aqueous 0.20 M sodium 4-toluenesulfonate solution as eluent. The ^{1}H NMR spectra of these isomers showed the proton in the 2-position on the imidazole ring to be shifted considerably upfield, due to shielding by the adjacent pyridine rings of two different bipyridyl ligands. This proved to be a useful handle in the identification of the two isomers, as this proton occurs at 5.98 ppm in the *rac* isomer and 5.68 ppm in the *meso* isomer due to the greater extent of the shielding effect in the latter isomer. Fig. 2 shows the NMR spectra of (**9*rac***) and (**9*meso***) along with that of the crude mixture for comparison. For each isomer the ^{1}H NMR signals were readily grouped (Table 2) into the five separate pyridine rings [Py(a)–(d)] by means of 1D-TOCSY and/or 2D-COSY spectra but the specific rings within the structure could not be unambiguously distinguished.

Table 2 ^{1}H NMR chemical shift values[a] for (**9**) and (**10**) in CD_3CN

	H6(d)	H5(t)	H4(t)	H3(d)
9*rac*				
Py(a)	7.70	7.21	8.03	8.51
Py(b)	8.13	7.61	8.21	8.54
Py(c)	7.60	7.25	7.94	8.41
Py(d)	7.92	7.47	8.10	8.56
Py(e)	7.20	7.18	8.06	8.53
9*meso*				
Py(a)	8.31	7.61	8.17	8.62
Py(b)	7.93	7.44	8.12	8.61
Py(c)	7.66	7.22	8.04	8.50
Py(d)	7.70	7.25	7.98	8.40
Py(e)	7.72	7.26	8.00	8.37
10*meso*				
Py(a)	7.80	7.41	8.03	8.26
Py(b)	6.99	6.67	7.51	7.95
Py(c)	7.58	7.20	8.06	8.64
Py(d)	8.54	7.79	8.19	8.54
Py(e)	7.59	7.32	8.01	8.47

[a] For atom labelling, see Fig. 1.

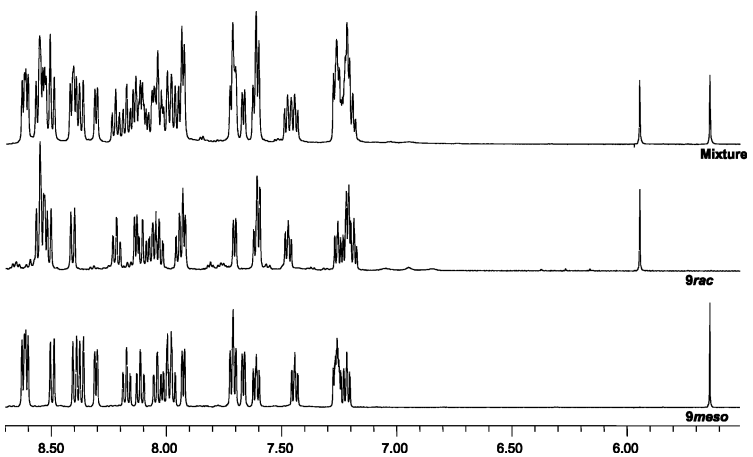

Fig. 2 NMR spectra of (**9**) showing the mixture and the two isomers after separation.

The structures of the two isomers were further confirmed by X-ray crystallography. In both cases it was possible to grow crystals suitable for X-ray diffraction by slow evaporation of an acetonitrile–toluene solution of the complex. The *rac* isomer (**9*rac***) crystallises as thin red plates in the chiral trigonal space group $P3_12_1$, with a full dinuclear cation in the asymmetric unit along with two full and two half PF_6^- anions, the latter lying on crystallographic two-fold rotation axes. The *meso* isomer (**9*meso***) crystallised as red needles in the triclinic space group $P\bar{1}$, with a full dinuclear cation in the asymmetric unit along with three PF_6^- anions (one being disordered), an acetonitrile and one and a half toluene solvate molecules (the last being disordered about a centre of inversion). Fig. 3 shows two perspective views of each isomer (**9*rac***) and (**9*meso***), which serves to show the very different shapes of these two stereoisomers.

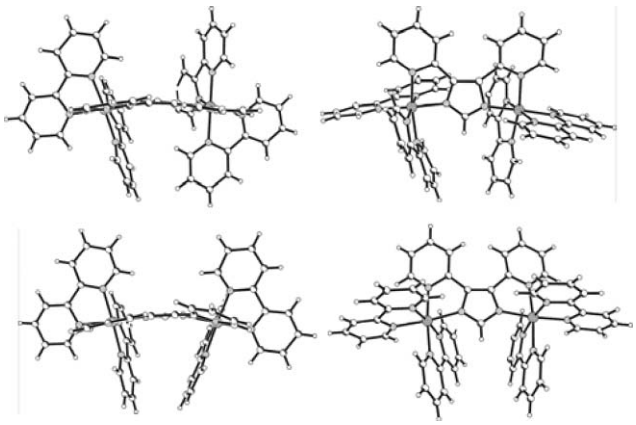

Fig. 3 Perspective views of (**9*rac***), top, and (**9*meso***), bottom.

When we attempted to synthesise dinuclear complexes of (**8**) we observed the formation of the *meso* isomer (**10*meso***) only. The X-ray crystal structure of this compound was also determined. It crystallises in the orthorhombic space group *Cmca* with the dinuclear cation lying on a crystallographic mirror plane passing through C2 of the imidazole ring and the attached phenyl ring. The asymmetric unit also contains two half PF_6^- anions (one on a two-fold rotation axis and the other on a mirror plane), two quarter PF_6^- anions (one on a site of 2/m symmetry) and a highly disordered toluene solvate molecule. A space-filling diagram of the dinuclear cation (**10*meso***) is shown in Fig. 4. This shows that the central phenyl ring is neatly sandwiched between two pyridine

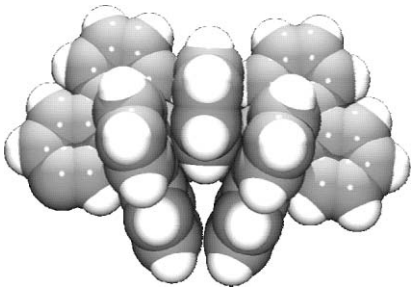

Fig. 4 Space-filling diagram of (**10*meso***).

rings of bpy ligands that are significantly bowed towards one another. This deformation results from a curvature of the bridging ligand which is substantially nonplanar. The selective formation of a single diastereoisomer is unusual for such complexes[15] and probably occurs in this case to maximise the observed π–π stacking of the aryl rings and minimise unfavourable steric interactions that would exist in the corresponding *rac* isomer.

Electrochemistry

In order to probe the metal–metal communication between the ruthenium centres in complexes (**9**) and (**10**) electrochemical studies were carried out. As noted above, the two diastereoisomers of complexes of ligands (**3**) and (**4**) were found to display unusually different K_c values. The corresponding complexes of ligands (**5**) and (**6**) have only been previously measured as mixtures of isomers and various values of K_c have been reported for the complexes of (**5**).[3] We therefore decided to separate these compounds into the *rac* and *meso* isomers and measure the K_c values of the individual isomers. The redox potentials for the complexes (**5*rac***), (**5*meso***), (**6*rac***) and (**6*meso***) are listed in Table 3. The K_c values for the two stereoisomers of the complexes of (**5**) are identical and at the high end of the range of values previously reported for the mixture of diastereoisomers.[3] The K_c values for (**6*rac***) and (**6*meso***) are significantly lower and do show a measurable difference between the two isomers. Table 3 also shows the results for the three complexes which are the focus of this study, along with data for $[Ru(bpy)_3]^{2+}$ as a comparison. Redox potentials of complexes (**9**) and (**10**) are cathodically shifted relative to $[Ru(bpy)_3]^{2+}$ due to the anionic nature of the bridging ligand.

For the three complexes (**9*rac***), (**9*meso***) and (**10*meso***) in $[(n\text{-}C_4H_9)_4N]PF_6$–$CH_3CN$ media we see a considerable separation

Table 3 Redox potentials and K_c values for the stereoisomers of compounds (**5**), (**6**), (**9**) and (**10**) compared to $Ru(bpy)_3^{2+}$

Compound	Electrolyte	ΔE_{ox}[a]	E_{ox2}	E_{ox1}	E_{red1}	E_{red2}	E_{red3}	K_c[b]
5*rac*	PF_6^-	212	1244	1032	−1048	−1560	−1888	3830
5*meso*	PF_6^-	212	1256	1044	−1044	−1540	−1900	3830
6*rac*	PF_6^-	168	1208	1040	−892	−1524	−1920	690
6*meso*	PF_6^-	160	1220	1060	−876	−1500	−1924	506
9*rac*	PF_6^-	349	884	540	−1800	−2064	−2548	652 000
9*meso*	PF_6^-	312	844	532	−1824	−2052	−2528	188 000
10*meso*	PF_6^-	276	836	560	−1816	−2153	—	46 200
9*rac*	$B(C_6F_5)_4^-$	347	931	584	−1832	−2310	—	733 000
9*meso*	$B(C_6F_5)_4^-$	341	941	592	−1840	−2104	—	793 000
$[Ru(bpy)_3]^{2+}$	PF_6^-	—	—	950	−1640	−1820	−2080	—

[a] $\Delta E_{ox} = E_{ox2} - E_{ox1}$. [b] Comproportionation constant, $K_c = \exp\{\Delta E_{ox}F/RT\}$, where F/RT takes the value 38.92 V^{-1} at 298 K.

This journal is © The Royal Society of Chemistry 2006

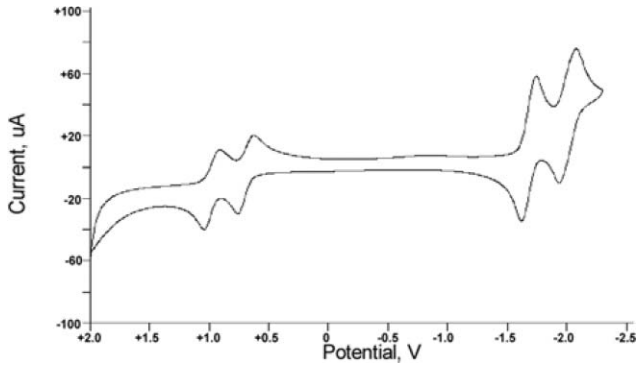

Fig. 5 Cyclic voltammogram of (**10*meso***) (0.1 M $[(n\text{-}C_4H_9)_4N]PF_6$–$CH_3CN$: Pt working electrode; *vs.* $FeCp_2^+/FeCp_2^0$).

between the redox couples associated with the first two reversible oxidation processes. Such separations are associated with high K_c values and thus we can infer a high degree of communication between the two metal centres. Fig. 5 shows the cyclic voltammogram for complex (**10*meso***), which is typical for these complexes. The magnitudes of the K_c values lie between those previously found for the corresponding complexes of ligands (**3**) and (**4**). Once again a significant difference is observed between the *rac* and *meso* isomers of (**9**).

A second set of measurements were carried out, again in acetonitrile solution, but this time using the electrolyte tetra(*n*-butyl)ammonium tetrakis(pentafluorophenyl)borate, $[(n\text{-}C_4H_9)_4N]B(C_6F_5)_4$.[16] Under these conditions, higher values of K_c were observed, but the K_c values for the diastereoisomers (**9*rac***) and (**9*meso***) were now very similar. The greater separation of the potentials associated with the oxidation processes, and the resultant higher K_c values, obtained in $B(C_6F_5)_4^-$ compared with PF_6^- media is not unexpected and reflects a higher association of the latter anion with the cations, which in turn lowers the potential of the oxidation processes.[5d] This lowering of the potential is more pronounced for the second oxidation process as the charges are greater, thus lowering ΔE_{ox}. In $B(C_6F_5)_4^-$ media, the association is very much less, and apparently does not differ significantly between the two diastereoisomers (**9*rac***) and (**9*meso***). The fact that a difference in ΔE_{ox} is observed between the diastereoisomers in PF_6^- media reflects the fact that where association is present, its extent is different between the diastereoisomers giving rise to different values of ΔE_{ox}.

It is interesting to note (Table 3) that the ΔE_{ox} values for the *rac* diastereoisomer (**9*rac***) are virtually the same in both media, whereas they differ significantly for the *meso* form (**9*meso***). This is consistent with the proposal that there is considerable ion association between the PF_6^- anion and the *meso* diastereoisomer in particular. This is the isomer with a substantially larger cavity, above and below the plane of the bridging ligand, that can accommodate the anion (Fig. 3).

A recent publication[17] has warned about the use of electrochemically-derived K_c values as a means of measuring metal–metal communication, due to the effect of ion pairing. In the present case, the differences in ΔE_{ox} (and therefore K_c) determined in the two media reflect differences in ion association rather than inter-metal communication. For even more strongly associating anions, such as 4-toluenesulfonate, the differential association can be quite profound, a fact that we actually use to our advantage when separating the two isomers by cation exchange chromatography.

For complexes (**9**) and (**10**) we see two $2e^-$ reversible reduction processes that correspond to reduction of two different bpy rings. With dinuclear ruthenium complexes containing π-deficient diazine bridging ligands, such as (**1**), (**5**) and (**6**), the first reduction usually involves electron transfer into the bridging ligand.[1,2] However, the imidazolate ring is a π-excessive system with a much higher energy LUMO orbital. Thus the bpy ligands are the first to be reduced. In compounds (**9*rac***) and (**9*meso***) a subsequent $1e^-$ reduction was observed that corresponds to reduction of the bridging ligand. When using the $B(C_6F_5)_4^-$ counterion, this reduction was beyond the limits of the solvent system.

Spectroelectrochemistry

The UV/Vis spectral properties of the 4+ forms of the complexes of (**3**) and (**4**) have been described previously,[7] but no spectroelectrochemical studies were carried out. As part of the present study, we have now recorded the UV/Vis/NIR spectra for the diastereoisomers of $(\mathbf{3})^{n+}$ and $(\mathbf{4})^{n+}$ $\{n = 4, 5, 6\}$ over the range 3050–30000 cm^{-1} (Table S1†). The spectral progression accompanying the oxidation of $(\mathbf{3}\textit{meso})^{4+}$ to $(\mathbf{3}\textit{meso})^{5+}$ in 0.1 M $[(n\text{-}C_4H_9)_4N]PF_6$–$CH_3CN$ at −35 °C is shown in Fig. 6(a). The lowest energy absorption bands in the spectra of the 4+ species are assigned as $d\pi(Ru) \rightarrow \pi^*(BL)$ MLCT transitions. These bands decreased in energy and intensity following one-electron oxidation to the mixed-valence (5+) species, and collapsed completely on further oxidation to the 6+ state. The new bands in the regions 3050–9000 cm^{-1} and 14000–16000 cm^{-1} in the mixed-valence species are assigned as IVCT and LMCT transitions, respectively. The former are absent in the spectra of the 6+ species, while the latter increase in intensity, and are consistent with the $\pi(bpy) \rightarrow d\pi(Ru^{III})$ LMCT transitions at 14815 and 17160 cm^{-1} in $[Ru^{III}(bpy)_3]^{3+}$.[18] Comparable behaviour was observed for $(\mathbf{3}\textit{rac})^{n+}$, and for the two diastereoisomers of $(\mathbf{4})^{n+}$.

The UV/Vis/NIR spectral properties for the diastereoisomers of $(\mathbf{9})^{n+}$ $\{n = 3, 4, 5\}$ in 0.1 M $[(n\text{-}C_4H_9)_4N]PF_6$–$CH_3CN$ and 0.02 M $[(n\text{-}C_4H_9)_4N]B(C_6F_5)_4$–$CH_3CN$ at −35 °C are reported in Table S2,† and the spectra of $(\mathbf{9}\textit{rac})^{n+}$ in PF_6^- media are shown in Fig. S1.† The MLCT transitions exhibited similar behaviour on oxidation to that described for $(\mathbf{3})^{n+}$ and $(\mathbf{4})^{n+}$. The mixed-valence (4+) state is characterised by two new bands in the regions 3050–8000 cm^{-1} and 8000–15000 cm^{-1} which are assigned as IVCT and LMCT transitions, respectively. Further oxidation to the 5+ species causes a disappearance of the IVCT band, and a blue-shift in the LMCT band. While the latter contradicts the expected red-shift in LMCT bands with oxidation, similar behaviour has been observed for other dinuclear ruthenium complexes incorporating anionic bridging ligands such as 3,5-bis(pyrazin-2-yl)-1,2,4-triazolate.[19] In contrast to $(\mathbf{3})^{n+}$ and $(\mathbf{4})^{n+}$ in which electron transfer involves a superexchange-assisted electron transfer mechanism *via* the π,π* bridging ligand orbitals, the lowest energy orbitals (LUMOs) of $(\mathbf{9})^{n+}$ lie relatively high in energy. As a result, hole transfer *via* the highest occupied molecular orbitals (HOMOs) of the bridging ligand is the dominant electron transfer pathway. These observations are corroborated by the electrochemical data which show that the first reduction is bpy-based

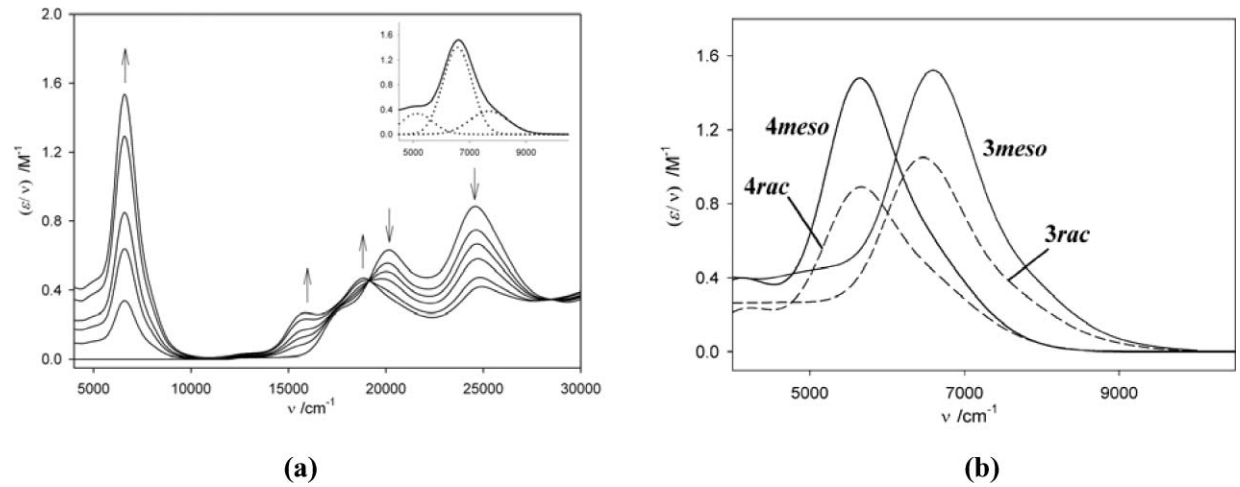

Fig. 6 (**a**) Spectral progression for the oxidation reaction $(\mathbf{3}meso)^{4+} \rightarrow (\mathbf{3}meso)^{5+}$ in 0.1 M $[(n\text{-}C_4H_9)_4N]PF_6$–$CH_3CN$ at −35 °C. The inset shows the best fit Gaussian deconvolution of the IVCT band. (**b**) NIR spectra for both isomers of $(\mathbf{3})^{5+}$ and $(\mathbf{4})^{5+}$ in 0.1 M $[(n\text{-}C_4H_9)_4N]PF_6$–$CH_3CN$ at −35 °C.

Table 4 NIR spectral data of the reduced absorption spectra (ε/ν *vs.* ν) for $(\mathbf{3})^{5+}$, $(\mathbf{4})^{5+}$ and $(\mathbf{9})^{4+}$ in 0.1 M $[(n\text{-}C_4H_9)_4N]PF_6$–$CH_3CN$ and $(\mathbf{9})^{5+}$ in 0.02 M $[(n\text{-}C_4H_9)_4N]B(C_6F_5)_4$–$CH_3CN$ at −35 °C

Electrolyte	Complex	$\nu_{max} \pm 10/cm^{-1}$	$(\varepsilon/\nu)_{max} \pm 0.0001/M^{-1}$	$\Delta\nu_{1/2}{}^{a} \pm 20/cm^{-1}$	$\Delta\nu_{1/2}{}^{\circ}/cm^{-1}$	M_0/M^{-1}	$H_{ab}{}^{d}/cm^{-1}$
PF_6^-	$\mathbf{3}meso^{5+}$	6590	1.5218	1470	3480	3211	3295
	$\mathbf{3}rac^{5+}$	6460	1.2737	1492	3440	2650	3230
	$\mathbf{4}meso^{5+}$	5625	1.4908	1346	3210	2538	2813
	$\mathbf{4}rac^{5+}$	5628	0.8995	1516	3215	1656	2814
	$\mathbf{9a}rac^{4+}$	4475	1.4816	1112[b]	2866	[c]	2238
	$\mathbf{9b}meso^{4+}$	4560	1.2061	1029[b]	2893	[c]	2280
$B(C_6F_5)_4^-$	$\mathbf{9a}rac^{4+}$	4120	0.9668	1148[b]	2750	[c]	2060
	$\mathbf{9b}\ meso^{4+}$	4105	0.9119	1160[b]	2745	[c]	2053

[a] $\Delta\nu_{1/2}{}^{\circ} = [1836(\nu_{max})]^{1/2}$ at 238 K.[20] [b] Bandwidth for the high-energy side of the IVCT manifold. The lower energy side was obscured at the detector limit. [c] The M_0 for the full band manifold could not be measured reliably. [d] H_{ab} determined as $\frac{1}{2}\nu_{max}$,[20] assuming that the complexes are delocalised (Class III).[21]

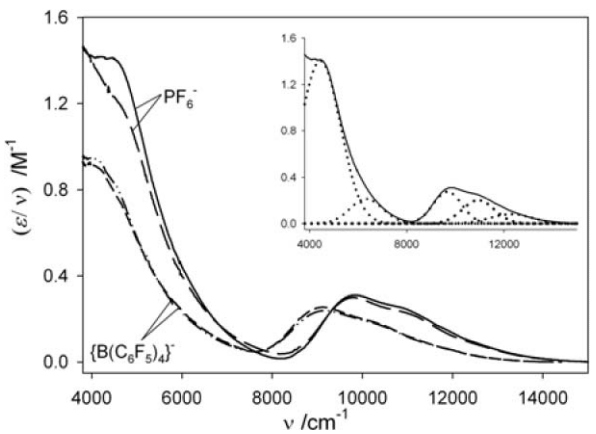

Fig. 7 NIR spectra for $(\mathbf{9})^{4+}$ in 0.1 M $[(n\text{-}C_4H_9)_4N]PF_6$–$CH_3CN$ {*meso* (—), *rac* (---)} and 0.02 M $[(n\text{-}C_4H_9)_4N]B(C_6F_5)_4$–$CH_3CN$ {*meso* (---), *rac* (-·-)} at −35 °C. The inset shows the best fit Gaussian deconvolution of $(\mathbf{7}rac)^{4+}$ in 0.1 M $[(n\text{-}C_4H_9)_4N]PF_6$–$CH_3CN$.

in $(\mathbf{9})^{n+}$, rather than bridging ligand-based as is the case for $(\mathbf{3})^{n+}$ and $(\mathbf{4})^{n+}$.

Fig. 6(b) shows the NIR bands for the diastereoisomers of $(\mathbf{3})^{5+}$ and $(\mathbf{4})^{5+}$ (in PF_6^- media), and Fig. 7 shows the NIR bands for the diastereoisomers of $(\mathbf{9})^{4+}$ (in PF_6^- and $B(C_6F_5)_4^-$ media). The energy (ν_{max}), intensity $\{(\varepsilon/\nu)_{max}\}$, bandwidth ($\Delta\nu_{1/2}$) and the band area (zeroth-moment, M_0) for the IVCT bands are reported in Table 4. The parameters for the bands obtained from Gaussian deconvolution of the manifolds are reported in Tables S2 (for $(\mathbf{3})^{5+}$ and $(\mathbf{4})^{5+}$) and S3 (for $(\mathbf{9})^{4+}$).† In each case, the IVCT bands were fitted by three Gaussian-shaped components, denoted IVCT(1), (2) and (3) in order of increasing energy; however IVCT(1) was obscured at the detector limit for $(\mathbf{9})^{4+}$. The LMCT bands for $(\mathbf{9})^{4+}$ were also fitted by three Gaussian components. For all complexes, IVCT(2) exhibited the highest intensity and dominated the IVCT manifold.

The three IVCT components arise due to separate electronic excitations from one of the three $d\pi_n$ (n = 1–3) orbitals at Ru^{II} to the hole in the corresponding $d\pi_n$ orbital which is present in any of the three spin–orbit states at Ru^{III}.[22] The magnitude of the separation between the components (*ca.* 1000 cm^{-1}) is consistent with the energy splittings between the three $d\pi_n$ orbitals which arise due to the combined effects of spin–orbit coupling ($\xi \sim 1100\ cm^{-1}$ for Ru^{III})[23] and ligand-field asymmetry. If the xy plane defines the plane of the bridging ligands and z lies perpendicular to the plane, the three $d\pi_n$ orbitals may be more closely represented by d_{xz}, $d_{yz}(d\pi_1, d\pi_2)$ and $d_{xy}(d\pi_3)$. The enhanced stabilisation of the former due to the relatively greater overlap with the π,π^* orbitals of

 This journal is © The Royal Society of Chemistry 2006

the bridging ligands, accounts for the higher intensity of IVCT(2) relative to IVCT(3).

For all complexes, the bandwidths are narrow compared with the theoretical predictions for $\Delta\nu_{1/2}^{\circ}$, which together with the significant intensity of the NIR manifolds suggest that the systems are delocalised (Class III). The IVCT components are more accurately assigned as transitions between bonding and non-bonding orbitals within the molecular orbital manifolds of the dinuclear complexes, as described within the three-state model of Ondrechen,[24] and illustrated schematically in Fig. S2.† For $(\mathbf{3})^{5+}$ and $(\mathbf{4})^{5+}$, the salient feature of the model is the $d\pi \rightarrow \pi^*(BL)$ energy gap, which is larger for the former due to its enhanced π-acceptor nature.[7] The relatively greater separation between the bonding and non-bonding orbitals is manifested as a blue-shift in the NIR band for $(\mathbf{3})^{5+}$ relative to $(\mathbf{4})^{5+}$. For delocalised mixed-valence complexes, the energy of the NIR transition provides a direct measure of the electronic coupling parameter, H_{ab} ($H_{ab} = \frac{1}{2}\nu_{max}$, Table 4).[22]

As shown in Table 4, the parameters of the NIR bands differ for the same diastereoisomer of $(\mathbf{3})^{5+}$ and $(\mathbf{4})^{5+}$, and between the two diastereoisomeric forms of the same complex. For both complexes, the integrated intensity of the manifold is greater for the *meso* relative to the *rac* forms. X-Ray structural studies[7] revealed comparable inter-metal distances for the diastereoisomers of $(\mathbf{3})^{5+}$ {6.016 Å for *meso*, 6.014 Å for *rac*} which would be similar for $(\mathbf{4})^{5+}$. The differences in the IVCT parameters between the diastereoisomers of the same complex are ascribed to differential ion-pairing interactions and specific solvation effects. The H_{ab} values suggest that for a given diastereoisomer, $(\mathbf{3})^{5+}$ exhibits greater electronic coupling relative to $(\mathbf{4})^{5+}$. The degree of aromaticity of the bridge has been postulated to facilitate electronic coupling between metal centres. The 1,2,5-oxadiazole system has a low degree of aromaticity and high "diene" character, with the electronegative oxygen atom contributing little of its electron density into the ring.[25] Since sulfur is less electronegative than oxygen and does not reduce the electron density of the ruthenium centres to the same extent, $(\mathbf{4})^{5+}$ would be expected to be a more delocalised system because of the greater polarisability of the larger sulfur atom. However, the relatively low aromatic character of the bridge in $(\mathbf{3})^{5+}$ has not restricted the electronic communication between the metals. In fact, the low aromatic character has served to enhance the electronic coupling, as exemplified by the higher H_{ab} values in $(\mathbf{3})^{5+}$.

While the diastereoisomers of $(\mathbf{9})^{4+}$ exhibit comparable band parameters to one another in each electrolyte system, the characteristics of the IVCT and LMCT bands are markedly dependent on the identity of the electrolyte counter-ion. In $B(C_6F_5)_4^-$ media, the IVCT bands are red-shifted and narrower and the parameters $(\varepsilon/\nu)_{max}$, M_0 and H_{ab} are decreased compared with their values in PF_6^- electrolyte. Ion-pairing effects have been shown to influence the IVCT characteristics in a number of dinuclear ruthenium[26] and iron[27] systems. Qualitatively, the experimental observations in the present study are similar to these previous literature reports which have shown that IVCT bands are blue-shifted in the presence of relatively strongly ion-pairing electrolytes (PF_6^- in the present case). The effect is attributed to ion-pair formation which induces an additional energy contribution to ν_{max}. The results show that in $(\mathbf{9})^{4+}$ the significant electronic communication between the metal centres is most likely to occur *via* the highest occupied molecular orbital HOMO of the bridging ligand, rather than the LUMO in the case of $(\mathbf{3})^{5+}$ and $(\mathbf{4})^{5+}$. In addition, the electronic coupling is enhanced in the presence of a stronger ion-pairing electrolyte (PF_6^-).

Conclusions

The results reported here show that it is not the inclusion of a heteroatom in the aromatic ring system that is inherently responsible for the amplification in metal–metal communication we observe in such systems. There is no obvious trend in the degree of communication as we move from imidazolate- to oxadiazole- to thiadiazole-bridge. It should perhaps be noted that the imidazolate bridge is in fact anionic, while both the oxadiazole and thiadazole are neutral and so care should be taken when making direct comparisons. Nevertheless, it would appear that the inclusion of a five-membered ring in the bridge is the most important factor for such strong inter-metal communication. Furthermore, beyond a broad consideration of intermetallic distances, it would not appear to be possible to accurately predict the extent of communication in any particular bridging ligand system.

Experimental

General

^{1}H NMR experiments were performed on a Varian INOVA 500 MHz NMR spectrometer at room temperature. ^{1}H NMR assignments were made with the assistance of 1D-TOCSY experiments to identify each pyridine ring spin system, while individual protons within a ring were assigned on the basis of their chemical shifts and the following typical ^3J coupling patterns for pyridine protons: H3 (d, $J = 8$ Hz), H4 (t, $J = 8$ Hz), H5 (dd, $J = 8$, 5 Hz), H6 (d, $J = 5$ Hz). Mass spectra were recorded using a Kratos MS80RFA mass spectrometer with a Mach 3 data system. Electron impact (EI) spectra were obtained at 70 eV with a source temperature of 250 °C. Electrochemical measurements were performed under argon using a Bioanalytical Systems BAS 100A Electrochemical Analyser. Cyclic and differential pulse voltammograms were recorded under Ar in 0.02 M $[(n\text{-}C_4H_9)_4N]B(C_6F_5)_4$–$CH_3CN$ at +25 °C using a glassy carbon working electrode, a platinum wire auxiliary electrode and an Ag/AgCl (0.02 M $[(n\text{-}C_4H_9)_4N]B(C_6F_5)_4$ in CH_3CN) reference electrode; or in 0.1 M $[(n\text{-}C_4H_9)_4N]PF_6$–$CH_3CN$ using an Ag/AgCl (0.1 M $[(n\text{-}C_4H_9)_4N]PF_6$ in CH_3CN) reference electrode. Ferrocene was added as an internal standard on completion of each experiment {the ferrocene/ferrocenium couple ($FeCp_2^+/FeCp_2^0$) occurred at +550 mV *vs.* Ag/AgCl}: all potentials are quoted in mV *versus* $FeCp_2^+/FeCp_2^0$.[15] Cyclic voltammetry was performed with a sweep rate of 100 mV s^{-1}; differential pulse voltammetry was conducted with a sweep rate of 4 mV s^{-1} and a pulse amplitude, width and period of 50 mV, 60 ms and 1 s, respectively. In order to obtain reasonable electrochemical response, measurements in the 0.02 mol dm^{-3} $[(n\text{-}C_4H_9)_4N]B(C_6F_5)_4$–$CH_3CN$ electrolyte required a concentration of complex which was approximately double that in 0.1 mol dm^{-3} $[(n\text{-}C_4H_9)_4N]PF_6$–$CH_3CN$.

Electronic spectra were recorded using a CARY 5E UV/Vis/NIR spectrophotometer interfaced to Varian WinUV software. The absorption spectra of the electrogenerated

mixed-valence complexes $(\mathbf{3})^{n+}$, $(\mathbf{4})^{n+}$ and $(\mathbf{9})^{n+}$ were obtained *in situ* by the use of an optically semi-transparent thin-layer electrosynthetic (OSTLE) cell mounted in the path of the spectrophotometer.[28] Solutions for the spectroelectrochemical experiments contained 0.1 M $[(n\text{-}C_4H_9)_4N]PF_6$ or 0.02 M $[(n\text{-}C_4H_9)_4N]B(C_6F_5)_4$ supporting electrolyte and the complex (*ca.* 0.5 mM) under investigation in acetonitrile. All experiments were conducted at −35 °C according to methods described previously.[29] The spectroelectrochemical experiments were conducted at low temperature to suppress the secondary chemical reactivity of the electrogenerated mixed-valence systems, and for enhanced spectral resolution. The near-infrared (NIR) spectra of the dinuclear systems were scaled[20a,30] as $\int\{\varepsilon(\nu)/\nu\}d\nu$ and deconvoluted by use of the software package GRAMS32.

2,2′-Pyridil (Aldrich), hexamethylenetetramine (Aldrich), benzaldehyde (Aldrich), $RuCl_3\cdot xH_2O$ (Strem, 99%), SP Sephadex C-25 (Amersham Pharmacia Biotech) and laboratory reagent solvents were used as received. $[Ru(bpy)_2Cl_2]\cdot 2H_2O$ was prepared according to the literature procedure.[31] Tetra-*n*-butylammonium hexafluorophosphate ($[n\text{-}C_4H_9)_4N]PF_6$; Fluka, 99+%) was dried *in vacuo* at 60 °C prior to use and acetonitrile (CH_3CN; Aldrich, 99.9+%) was distilled over CaH_2 before use. $[(n\text{-}C_4H_9)_4N]B(C_6F_5)_4$[16] was prepared by metathesis from lithium tetrakis(pentafluorophenyl)borate ($LiB(C_6F_5)_4.Et_2O$; Boulder Scientific) as described previously.[32]

Syntheses

Preparation of 4,5-di(2-pyridyl)imidazole. Hexamethylenetetramine (0.13 g, 9.27×10^{-4} mol) was added to a solution of 2,2′-pyridil (1.10 g, 5.18×10^{-3} mol) and a tenfold excess of ammonium acetate (4 g, 5.18×10^{-2} mol) in acetic acid (25 mL). The mixture was refluxed for 1 hour and subsequently allowed to cool to room temperature. The dark mixture was diluted with water (25 mL) and neutralised with ammonium hydroxide solution and was then filtered through Celite to yield a green solution. The green solution was extracted with CH_2Cl_2 (3 × 25 mL), the combined organic fractions were dried over sodium sulfate and the solvent removed to yield a dark tarry residue containing both the desired product and a second product containing an imidazolo[1,5-*a*]pyridine ring system. The mixture was purified by column chromatography on silica eluting with 10% MeOH in $CHCl_3$ to yield a pale brown oil which solidified on standing. Yield 0.15 g (13%). EI mass spectrum: calc. *m*/*z* for $C_{13}H_{10}N_4$ 222; found 221. ^{1}H NMR ($CDCl_3$) δ: 8.58 (2H, d, H6); 8.34 (2H, bs, H3); 7.73 (3H, m, H4, H2); 7.18 (2H, t, H5).

Preparation of 4,5-di(2-pyridyl)-2-phenylimidazole. Benzaldehyde (0.375 g, 3.53×10^{-3} mol) was added to a solution of 2,2′-pyridil (0.75 g, 3.53×10^{-3} mol) and ammonium acetate (2.72 g, 3.53×10^{-2} mol) in acetic acid (10 mL). The mixture was heated in a microwave for 5 minutes (5 × 1 minute with swirling of the flask between periods of heating). The reaction mixture was allowed to cool to room temperature and neutralised with conc. ammonia solution. The pale yellow precipitate that formed was collected and washed with water and a small amount of cold ethanol, to afford the desired product in 46% yield (0.48 g). EI mass spectrum: calc. *m*/*z* for $C_{19}H_{14}N_4$ 298; found 297. ^{1}H NMR ($CDCl_3$) δ: 8.60 (2H, d, H6); 8.33 (2H, br s, H3); 8.02 (2H, d, H*ortho*); 7.83 (2H, t, H4); 7.45 (2H, t, H*meta*); 7.38 (1H, t, H*para*); 7.20 (2H, t, H5).

Preparation and separation of *rac*- and *meso*-$[(bpy)_2Ru(\mu\text{-}7)Ru(bpy)_2](PF_6)_3$, (9*rac*) and (9*meso*). $[Ru(bpy)_2Cl_2]\cdot 2H_2O$ (66.0 mg, 1.28×10^{-4} mol) was added to a suspension of 4,5-di(2-pyridyl)imidazole (19.0 mg, 6.38×10^{-5} mol) in ethylene glycol (2.5 mL) and 2 drops of conc. NaOH. The mixture was heated in a microwave for 2 minutes in 20–30 second intervals swirling the flask between each period of heating. The dark red-brown mixture was cooled to room temperature and water (5 mL) added. The desired complex was isolated as the hexafluorophosphate salt by addition of an excess of an aqueous saturated ammonium hexafluorophosphate solution. The dark precipitate was collected by suction filtration and washed with water. The complex was purified by converting to the chloride salt by stirring in water with Amberlite resin IRA-400(Cl) for 20 minutes and any mononuclear compound removed by gradient elution on SP Sephadex C-25 with NaCl solution (0.125 M–0.50 M). The product was precipitated by addition of saturated ammonium hexafluorophosphate solution, and collected by filtration.

The *rac* and *meso* isomers were readily separated by cation exchange chromatography. The hexafluorophosphate salt was converted to the chloride salt by stirring in water with excess Amberlite anion exchange resin. The aqueous solution was loaded on a Sephadex column and eluted with 0.2 M sodium 4-toluenesulfonate solution, the *rac* isomer being eluted first. The two red fractions were precipitated by addition of potassium hexafluorophosphate. The resultant solids were purified by dissolution in acetone and adsorption on a short silica plug, washed with water and acetone, and then removed from the silica gel with a 5% solution of ammonium hexafluorophosphate in acetone. The complexes were isolated by the addition of water and partial removal of the solvent under reduced pressure. The red precipitate that formed was collected by filtration and dried *in vacuo.* Yield, 72.8 mg (3.31×10^{-5} mol, 77%). For NMR data see Fig. 2 and Table 2.

Preparation of $[(bpy)_2Ru(\mu\text{-}8)Ru(bpy)_2](PF_6)_3$, (10*meso*). $[Ru(bpy)_2Cl_2]\cdot 2H_2O$ (55.0 mg, 1.07×10^{-4} mol) was added to a suspension of 4,5-di(2-pyridyl)-2-phenylimidazole (13.5 mg, 4.53×10^{-5} mol) in ethylene glycol (2.5 mL) and 2 drops of conc. NaOH added. The mixture was heated in a microwave for 2 minutes in 20–30 second intervals swirling the flask between each heating. The dark red brown mixture was cooled to room temperature and water (5 mL) added. The desired complex was isolated as the hexafluorophosphate salt by addition of an excess of an aqueous saturated ammonium hexafluorophosphate solution. The dark precipitate was collected by suction filtration and washed with water. The crude compound was first purified by column chromatograph on alumina using 10% MeOH in $CHCl_3$ as the eluent. The complex was separated from any mononuclear species or free ligand by conversion to the chloride salt with Amberlite resin IRA-400(Cl) for 20 minutes. Any mononuclear compound was removed by gradient elution on Sephadex SP C-25 with NaCl solution (0.125 M–0.50 M). The product was precipitated by addition of saturated ammonium hexafluorophosphate solution, and collected by filtration. The red precipitate was dissolved in a small amount of acetone, which was adsorbed onto a short silica column, washed with water

This journal is © The Royal Society of Chemistry 2006

Table 5 X-Ray crystal data

Compound	**9*rac***	**9*meso***	**10*meso***
Formula	$C_{53}H_{41}F_{18}N_{12}OP_3Ru_2$	$C_{65.5}H_{56}F_{18}N_{13}P_3Ru_2$	$C_{62.5}H_{49}F_{18}N_{12}P_3Ru_2$
Formula weight	1499.03	1662.28	1605.19
Crystal system	Trigonal	Triclinic	Orthorhombic
a/Å	14.031(1)	12.585(6)	26.890(2)
b/Å	14.031(1)	13.339(7)	11.609(1)
c/Å	54.000(10)	22.104(12)	43.684(3)
α/°	90	73.085(9)	90
β/°	90	81.326(10)	90
γ/°	120	62.856(9)	90
V/Å^3	9206(2)	3159(3)	13636(2)
Space group	$P3_12_1$	$P\bar{1}$	*Cmca*
Z	6	2	8
D_c/Mg m^{-3}	1.622	1.748	1.564
$F(000)$	4476	1670	6424
T/K	163(2)	93(2)	163(2)
Crystal form	Red plate	Red needle	Red rod
μ/mm^{-1}	0.674	0.664	0.611
$2\theta_{max}$/°	50	50	50
Data collected	63993	22821	47350
Unique data	10749	10548	6166
Parameters	822	962	516
R^a [$I > 2\sigma(I)$]	0.0560	0.0860	0.0826
wR^b (all data)	0.0849	0.2176	0.2551

^{a} $R = \sum(|F_o| - |F_c|)/\sum|F_o|$. ^{b} $wR = (\sum[w(F_o^2 - F_c^2)^2]/\sum[w(F_o^2)^2])^{1/2}$.

(4 mL) and removed from the silica gel with a 5% solution of ammonium hexafluorophosphate in acetone. Water was added to the complex-containing acetone solution and the solvent partially removed under reduced pressure. The residue was then collected by filtration, washed with water and dried under vacuum. Yield 31.1 mg (1.99×10^{-5} mol, 44%). For NMR data see Table 2.

X-Ray crystallography

The crystal data, data collection and refinement parameters for compounds (**9*rac***), (**9*meso***) and (**10*meso***) are given in Table 5. Measurements were made with a Siemens CCD area detector using graphite monochromatised Mo-Kα ($\lambda = 0.71073$ Å) radiation. The intensities were corrected for Lorentz and polarisation effects and for absorption.[33] The structures were solved by direct methods using SHELXS,[34] and refined on F^2 using all data by full-matrix least-squares procedures using SHELXL-97.[35] Due to the weakness of the data from these small crystals many of the atoms in each structure were restrained to approximate to isotropic behaviour. Hydrogen atoms were included in calculated positions with isotopic displacement parameters 1.2 times the isotropic equivalent of their carrier carbon atoms. The functions minimised were $\sum w(F_o^2 - F_c^2)$, with $w = [\sigma^2(F_o^2) + aP^2 + bP]^{-1}$, where $P = [\max(F_o)^2 + 2F_c^2]/3$.

CCDC reference numbers 271748–271750.

For crystallographic data in CIF or other electronic format see DOI: 10.1039/b514976m

Acknowledgements

We thank the Australian Research Council, the Royal Society of New Zealand Marsden Fund and the University of Canterbury for financial support of this work.

References

1 (*a*) P. J. Steel, *Coord. Chem. Rev.*, 1990, **106**, 227; (*b*) A. Juris, V. Balzani, F. Barigelletti, S. Campagna, P. Belser and A. von Zelewsky, *Coord. Chem. Rev.*, 1988, **84**, 85; (*c*) S. Swavey and K. J. Brewer, in *Comprehensive Coordination Chemistry II*, ed. J. A. McCleverty and T. J. Meyer, Elsevier, Oxford, 2004, vol. 1, p. 135.
2 V. Balzani, A. Juris, M. Venturi, S. Campagna and S. Serroni, *Chem. Rev.*, 1996, **96**, 759.
3 C. Kaes, A. Katz and M. W. Hosseini, *Chem. Rev.*, 2000, **100**, 3553.
4 (*a*) D. P. Rillema and K. B. Mack, *Inorg. Chem.*, 1982, **21**, 3849; (*b*) S. D. Ernst and W. Kaim, *Inorg. Chem.*, 1989, **28**, 1520; (*c*) D. A. Reitsma and F. R. Keene, *J. Chem. Soc., Dalton Trans.*, 1993, 2859.
5 (*a*) S. D. Ernst, W. Kasack and W. Kaim, *Inorg. Chem.*, 1988, **27**, 1146; (*b*) L. S. Kelso, D. A. Reitsma and F. R. Keene, *Inorg. Chem.*, 1996, **35**, 5144; (*c*) K. Kalyanasundaram and Md. K. Nazeeruddin, *Inorg. Chem.*, 1990, **29**, 1888; (*d*) B. D. Yeomans, L. S. Kelso, P. A. Tregloan and F. R. Keene, *Eur. J. Inorg. Chem.*, 2001, 239.
6 (*a*) C. Richardson and P. J. Steel, *Dalton Trans.*, 2003, 992; (*b*) D. M. D'Alessandro, F. R. Keene, P. J. Steel and C. J. Sumby, *Aust. J. Chem.*, 2003, **56**, 657; (*c*) A. J. Downard, I. G. Phillips and P. J. Steel, *Aust. J. Chem.*, 2004, **57**, 865; (*d*) P. J. Steel, *Molecules*, 2004, **9**, 440; (*e*) P. J. Steel, *Acc. Chem. Res.*, 2005, **38**, 243.
7 C. Richardson, P. J. Steel, D. M. D'Alessandro, P. C. Junk and F. R. Keene, *J. Chem. Soc., Dalton Trans.*, 2002, 2775.
8 G. Denti, S. Campagna, L. Sabatino, S. Serroni, M. Ciano and V. Balzani, *Inorg. Chem.*, 1990, **29**, 4750.
9 I. G. Phillips and P. J. Steel, *Aust. J. Chem.*, 1998, **51**, 371.
10 W. Langenbeck, G. Reinisch and K. Schonzart, *Chem. Ber.*, 1959, **92**, 2040.
11 J. Wang, R. Mason, D. VanDerveer, K. Feng and X. R. Bu, *J. Org. Chem.*, 2003, **68**, 5415.
12 S. E. Wolkenberh, D. D. Wisnoski, W. H. Leister, Y. Wang, Z. Zhao and C. W. Lindsley, *Org. Lett.*, 2004, **6**, 1453.
13 J. Elguero, C. Marzin, A. R. Katritzky and P. Linda, The Tautomerism of Heterocycles, *Adv. Heterocycl. Chem.*, Suppl. 1, 1976.
14 N. C. Fletcher, P. C. Junk, D. A. Reitsma and F. R. Keene, *J. Chem. Soc., Dalton Trans.*, 1998, 133.
15 F. R. Keene, *Chem. Soc. Rev.*, 1998, **27**, 185.
16 R. LeSuer and W. E. Geiger, *Angew. Chem., Int. Ed.*, 2000, **39**, 248.
17 D. M. D'Alessandro and F. R. Keene, *Dalton Trans.*, 2004, 3950.

18 K. Kalyanasundaram, S. M. Zakeeruddin and M. K. Nazeeruddin, *Coord. Chem. Rev.*, 1994, **132**, 259.
19 (*a*) R. Hage, A. H. J. Dijkhuis, J. G. Haasnoot, R. Prins, J. Reedijk, B. E. Buchanan and J. G. Vos, *Inorg. Chem.*, 1988, **27**, 2185; (*b*) R. Hage, J. G. Haasnoot, H. A. Nieuwenhuis, J. Reedijk, D. J. A. De Ridder and J. G. Vos, *J. Am. Chem. Soc.*, 1990, **112**, 9245; (*c*) L. De Cola, F. Barigelletti, V. Balzani, R. Hage, J. G. Haasnoot, J. Reedijk and J. G. Vos, *Chem. Phys. Lett.*, 1991, **178**, 491; (*d*) R. Hage, J. G. Haasnoot, J. Reedijk, R. Wang and J. G. Vos, *Inorg. Chem.*, 1991, **30**, 3263; (*e*) H. P. Hughes, D. Martin, S. Bell, J. J. McGarvey and J. G. Vos, *Inorg. Chem.*, 1993, **32**, 4402.
20 (*a*) N. S. Hush, *Prog. Inorg. Chem.*, 1967, **8**, 391; (*b*) N. S. Hush, *Electrochim. Acta*, 1968, **13**, 1005.
21 M. B. Robin and P. Day, *Adv. Inorg. Chem. Radiochem.*, 1967, **10**, 247.
22 K. D. Demadis, C. M. Hartshorn and T. J. Meyer, *Chem. Rev.*, 2001, **101**, 2655.
23 E. M. Kober and T. J. Meyer, *Inorg. Chem.*, 1983, **22**, 1614.
24 (*a*) L.-T. Zhang, J. Ko and M. J. Ondrechen, *J. Phys. Chem.*, 1989, **93**, 3030; (*b*) L. J. Root and M. J. Ondrechen, *Chem. Phys. Lett.*, 1982, **93**, 421; (*c*) J. Ko and M. J. Ondrechen, *Chem. Phys. Lett.*, 1984, **112**, 507; (*d*) M. J. Ondrechen, J. Ko and L. J. Root, *J. Phys. Chem.*, 1984, **88**, 5919; (*e*) J. Ko and M. J. Ondrechen, *J. Am. Chem. Soc.*, 1985, **107**, 6161; (*f*) M. J. Ondrechen, J. Ko and L.-T. Zhang, *J. Am. Chem. Soc.*, 1987, **109**, 1672; (*g*) L.-T. Zhang, J. Ko and M. J. Ondrechen, *J. Am. Chem. Soc.*, 1987, **109**, 1666.
25 G. P. Bean, *J. Org. Chem.*, 1998, **63**, 2497.
26 (*a*) M. D. Lowery, W. S. Hammack, H. G. Drickamer and D. N. Hendrickson, *J. Am. Chem. Soc.*, 1987, **109**, 8019; (*b*) J. T. Hupp, G. A. Neyhart, T. J. Meyer and E. M. Kober, *J. Phys. Chem.*, 1992, **96**, 10820; (*c*) N. A. Lewis, Y. S. Obeng and W. L. Purcell, *Inorg. Chem.*, 1989, **28**, 3796; (*d*) N. A. Lewis and Y. S. Obeng, *J. Am. Chem. Soc.*, 1988, **110**, 2306; (*e*) D. M. D'Alessandro, P. C. Junk and F. R. Keene, *Supramol. Chem.*, 2005, **17**, 529.
27 (*a*) P. Pereztejeda, P. Neto-Ponce and F. Sánchez, *J. Chem. Soc., Dalton Trans.*, 2001, 1686; (*b*) R. L. Blackbourn, Y. Dong, L. A. Lyon and J. T. Hupp, *Inorg. Chem.*, 1994, **33**, 4446.
28 C. M. Duff and G. A. Heath, *Inorg. Chem.*, 1991, **30**, 2528.
29 D. M. D'Alessandro and F. R. Keene, *Chem. Eur. J.*, 2005, **11**, 3679.
30 J. R. Reimers and N. S. Hush, *Inorg. Chem.*, 1990, **29**, 3686.
31 B. P. Sullivan, D. J. Salmon and T. J. Meyer, *Inorg. Chem.*, 1978, **17**, 3334.
32 D. M. D'Alessandro and F. R. Keene, *Chem. Phys.*, 2005, in the press.
33 G. M. Sheldrick, *SADABS*, University of Göttingen, Germany, 1998.
34 G. M. Sheldrick, *Acta Crystallogr., Sect. A*, 1990, **46**, 467.
35 G. M. Sheldrick, *SHELXL-97*, University of Göttingen, Germany, 1997.

 This journal is © The Royal Society of Chemistry 2006